Journal of Iberian Geology
https://doi.org/10.1007/s41513-021-00181-0

RESEARCH PAPER

Weathering events recorded in uppermost Hauterivian–lower Barremian clay-dominated continental successions from the NW Iberian Range: climatic vs. tectonic controls

Elisa Laita[1] · Blanca Bauluz[1] · Marcos Aurell[1] · Beatriz Bádenas[1] · Alfonso Yuste[1]

Received: 3 September 2021 / Accepted: 15 November 2021

Abstract
The facies and clay mineral study of clay/marl-rich levels from the Torrelapaja Formation (latest Hauterivian–early Barremian, NW Iberian Range, NE Spain) allowed to establish the palaeoclimatic and palaeoenvironmental conditions under they were generated. The muddy levels and pisoids contained therein of two logs were sampled and studied by X-ray diffraction and optical and electron microscopy. A similar mineralogical upwards trend is recorded in both logs, with a decrease in calcite coupled with an increase in quartz and orthoclase content and constant proportions in goethite, hematite, diaspore, anatase, rutile, ilmenite, and clay mineral content. The lower muddy levels have higher kaolinite content than the upper levels, where illitic phases are the dominant clay minerals. Smectite and intergrowths of illitic phases and kaolinite are also detected upwards. The kaolinite and smectite textures indicate an authigenic origin, whereas the illitic phases are former phases acting as a substrate for kaolinite crystallization. Pisoids mineralogy and texture show an in-situ origin, but some are fractured, indicating reworking processes. The mineral association found in the muddy levels is characteristic of oxisols formed under warm and humid conditions. The upward decrease in kaolinite content is coeval with an increase in the illitic phases and quartz content, related to siliciclastic input, but is also coeval with the presence of authigenic smectite. This indicates a decrease in chemical weathering, not fully registered due to the siliciclastic contribution, which was possibly associated with a change to colder, drier conditions during the latest Hauterivian–early Barremian in the studied area.

Keywords Illitic phases · Kaolinite · Palaeoclimate · Palaeosols · Weathering

Eventos de meteorización registrados en sucesiones continentales arcillosas del Hauteriviense superior-Barremiense inferior del NW de la Cordillera Ibérica: control climático vs. tectónico

Resumen
El estudio de facies y minerales de la arcilla de nieles de arcillas/margas de la Formación Torrelapaja (Hauteriviense superior–Barremiense inferior, NW Cordillera Ibérica, NE España) ha permitido establecer el paleoclima y el paleoambiente bajo las que se formaron. Se muestrearon y estudiaron por difracción de rayos X y microscopía óptica y electrónica los niveles de arcillas/margas y los pisoides que contienen dos afloramientos. Se observa una tendencia mineralógica similar hacia el techo en ambos afloramientos, con un descenso en el contenido en calcita junto a un aumento del de cuarzo y ortoclasa y proporciones constantes de goethita, hematites, diásporo, anatasa, rutilo, ilmenita y minerales de la arcilla. Los niveles inferiores tienen mayor contenido en caolinita que los niveles superiores, en los que las fases illíticas son los minerales de la arcilla

✉ Elisa Laita
laita@unizar.es

[1] IUCA-Department of Earth Sciences, Faculty of Sciences, Universidad de Zaragoza, Pedro Cerbuna 12, 50009 Zaragoza, Spain

Published online: 01 December 2021

dominante. Hacia el techo se detectan esmectita e interestratificados de fases illíticas y caolinita. La textura de la caolinita y la esmectita indican un origen autigénico, mientras que las fases illíticas son fases previas que actúan como substrato para la cristalización de la caolinita. La mineralogía y textura de los pisoides indican un origen in-situ, pero algunos están fracturados, indicando procesos de retrabajamiento. La asociación mineral presente en los niveles inferiores es características de oxisoles, formados bajo condiciones climáticas cálidas y húmedas. El descenso del contenido en caolinita hacia techo es coetáneo con el aumento en el contenido en fases illíticas y cuarzo, relacionado con el aporte de detríticos, pero también es coetáneo con la presencia de esmectita autigénica. Esto indica una disminución en la meteorización química, no completamente registrada debido al aporte detrítico, que posiblemente se asocie con un cambio hacia condiciones más frías y secas durante el Hauteriviense superior–Barremiense inferior en el área estudiada.

Palabras clave Caolinita · Fases illíticas · Meteorización · Paleoclima · Paleosuelos

1 Introduction

The study of the soils that formed in the landscapes of the past (i.e., palaeosols) provides key data for palaeoclimatic and palaeoenvironmental reconstructions (Mack et al., 1993). The formation of soils takes place near the Earth's surface in the contact among lithosphere, atmosphere, hydrosphere, and biosphere (Tabor et al., 2017), and the weathering processes that generate them are subject to strong climatic control. For this reason, the study of the mineral phases formed during soil formation, such as clay minerals and oxides, is of great interest, since they directly provide information about the climate and environment (Chamley, 1989; Do Campo et al., 2018; Laita et al., 2020; Sheldon & Tabor, 2009; Varela et al., 2018).

In this way, the variations in the clay mineral assemblages have been used as palaeoclimatic and palaeoenvironmental proxies for palaeosols developed in continental sequences. Those of Mesozoic sequences have been described by several authors (e.g., Bauluz et al., 2014; Do Campo et al., 2010, 2018; Ehrmann et al., 2005; Föllmi, 2012; Laita et al., 2020; Raucskik & Varga, 2008 and references therein).

Under humid subtropical to tropical conditions, intense chemical weathering produces very effective hydrolysis, which gives rise to oxisols (commonly known as laterites), where kaolinite is the main clay mineral along with aluminium hydroxides and Fe oxyhydroxides (Chamley, 1989; Do Campo et al., 2018; Mack et al., 1993; Righi & Meunier, 1995; Velde, 1995). By contrast, under dry and cold climates, the production of clay minerals depends on physical weathering because of the absence of significant hydrolysis (Chamley, 1989). These conditions enhance the genesis of gleysols, where the clay mineral assemblages are essentially dominated by smectite and illite (Dhillon & Dhillon, 1991; Do Campo et al., 2018). Gleysols are formed under dysoxic or anoxic conditions that give rise to redoximorphic features and gleyed horizons generated by the influence of the shallow or fluctuating groundwater table, which inhibits drainage and creates low-oxygen conditions (Tabor et al., 2017).

In Western Europe, the presence of ferruginous palaeosols including kaolinite indicates warm and humid conditions during the late Hauterivian–early Barremian (Bárdossy, 1982; Föllmi, 2012; Wright et al., 2000). On the other hand, Haywood et. al. (2004) have described an alternation of wet and dry seasons during the early Barremian in the west of Europe.

Within the Iberian Plate, a seasonal subtropical climate has been described during the Lower Cretaceous in the Iberian Range (NE Spain) (Bauluz et al., 2014; Buscalioni & Fregenal-Martínez, 2010). This climate is evidenced by the presence of kaolinite-rich clays, bauxites, and lateritic clays in several areas of the Iberian Plate (Bauluz et al., 2014; Combes, 1990; Laita et al., 2020; Molina & Salas, 1993; Yuste et al., 2015, 2017, 2020). By contrast, Laita et. al. (2020) also pointed out a change from warm/humid to cold/dry conditions in Barremian continental successions from the NW Maestrazgo Basin (SE Iberian Range), which are age-equivalent with some of the palaeosols levels studied in this work.

Usually, clay-rich sediments, rocks, and palaeosols include authigenic clay minerals, but they may also contain diagenetic clays. This must be borne in mind when using clay mineral assemblages as palaeoclimatic and palaeoenvironmental indicators, since diagenetic processes may transform clay minerals and invalidate their use as palaeoclimatic proxies (Bauluz et al., 2014; Dera et al., 2009). To evaluate the origin of the clays and rule out a possible diagenetic imprint, it is necessary to carry out thorough microtextural studies.

Considering all the above mentioned, this study applies a combination of facies analysis and the study of the clay mineralogy of clay/marl-rich outcrops of uppermost Hauterivian–lower Barremian continental successions located in the Torrelapaja subbasin (NE Spain) to evaluate their usefulness as a palaeoclimate indicator. The main aims of this research are: (1) to determine whether the clay minerals are authigenic, as a consequence of the edaphic process, detrital (inherited from the source area), or diagenetic; and (2) to examine the vertical and lateral variations in the clay mineralogy and their relationships with the palaeoenvironmental conditions, or other controlling factors, to deduce the palaeoclimate during the latest Hauterivian–early Barremian in this area of the Iberian Range (NE Spain).

2 Geological setting

2.1 Stratigraphic context

The progressive opening of the Atlantic Ocean and the westward propagation of the Tethys Ocean during the Late Jurassic-Early Cretaceous generated a rifting process in the Iberian Basin located in the eastern part of the Iberian Plate (e.g., Salas et al., 2001). The resulting extensional fault activity gave rise to the compartmentalization of the Basin into a set of subsident basins, subbasins and troughs (Aurell, Bádenas, et al., 2019a; Aurell, Fregenal-Martínez, et al., 2019b; Liesa et al., 2019). One of these subsiding basins was the Cameros Basin, a wide Late Jurassic–Early Cretaceous sedimentary domain located in the northwestern part of this rifting system, in the northwestern Iberian Range (Fig. 1a) (e.g., Casas-Sainz, 1993; Clemente, 2010; Gómez-Fernández & Meléndez, 1994; Mas et al., 2004, 2019). The high subsidence rates recorded in this basin during the Late Jurassic-Early Cretaceous rifting episode allowed the accumulation of more than 8000 m of continental and coastal sediments in its depocentral areas (Casas-Sainz et al., 2009).

The uppermost Hauterivian–lower Barremian succession studied here accumulated in the so-called Torrelapaja subbasin, located at the southeastern edge of the Cameros Basin (Fig. 1b). In this area, the Upper Jurassic–Lower Cretaceous synrift sedimentary record encompasses a 100–500 m-thick, terrigenous, calcareous succession that is divided into three synrift sequences (SS-1, SS-2,

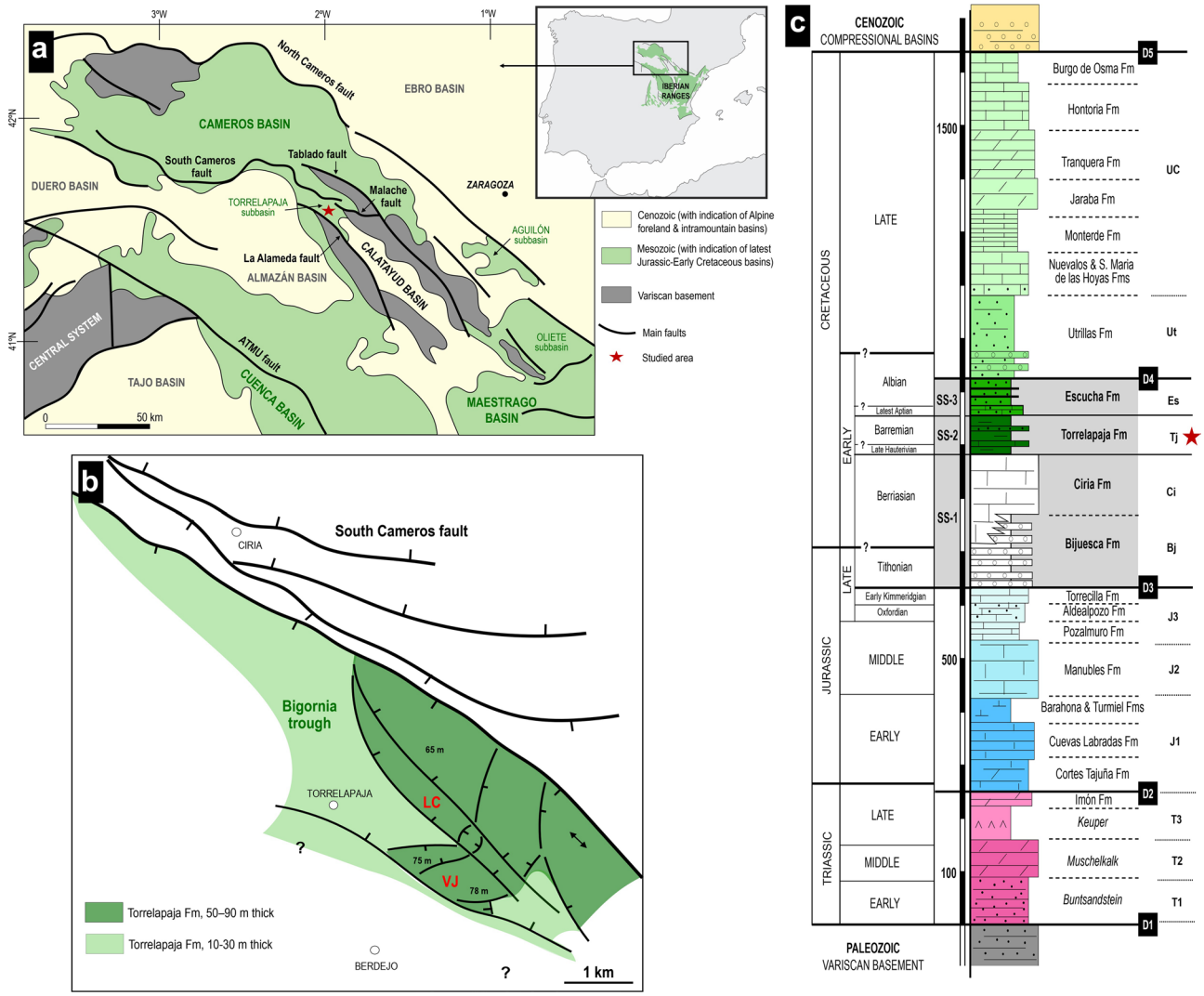

Fig. 1 **a** Geological location of the studied Torrelapaja subbasin at the SE edge of the Cameros Basin (slightly modified from Aurell et al., 2021); **b** Reconstruction of the sedimentation area during synrift sequence 2, showing the location of the studied logs (slightly modified from Aurell et al., 2021); **c** Summary of the Mesozoic sedimentary units indicating the distribution of the Lower Cretaceous synrift sequences in grey. The red star indicates the studied unit (slightly modified from Aurell et al., 2021)

and SS-3 in Fig. 1c; Aurell et al., 2021). SS-1 (middle Tithonian–middle Berriasian) is composed of continental deposits, including the terrigenous alluvial deposits of the Bijuesca Formation and the lacustrine-palustrine carbonates of the Ciria Formation. SS-2 (uppermost Hauterivian–lower Barremian) includes the continental mixed (terrigenous-carbonate) Torrelapaja Formation. SS-3 (middle–upper Albian) corresponds to the Escucha Formation and includes terrigenous-carbonate continental to coastal successions (Aurell et al., 2021).

The continental Torrelapaja Fm (SS-2), studied in this work, is an up-to-80 m-thick succession of muddy facies, limestones, sandstones, and conglomerates that accumulated preferentially in the so-called Bigornia Trough of the Torrelapaja subbasin (Fig. 1 and 2). The latest Hauterivian–early Barremian age of this unit was dated based on the presence of charophytes (Aurell et al., 2021; Martín-Closas, 1989). The boundary with the underlying Ciria Formation is a major angular unconformity, which is associated with a stratigraphic gap that encompasses the late Berriasian, the Valanginian and most of the Hauterivian. An irregular karstic surface is observed on top of the lacustrine limestones of the Ciria Formation. This occasionally presents multiepisodic filling, allowing the preservation of a rich assemblage of vertebrate remains (Aurell et al., 2021).

2.2 Sedimentological context

A facies analysis of the continental Torrelapaja Fm in the Bigornia Trough was performed by Aurell et. al. (2021),

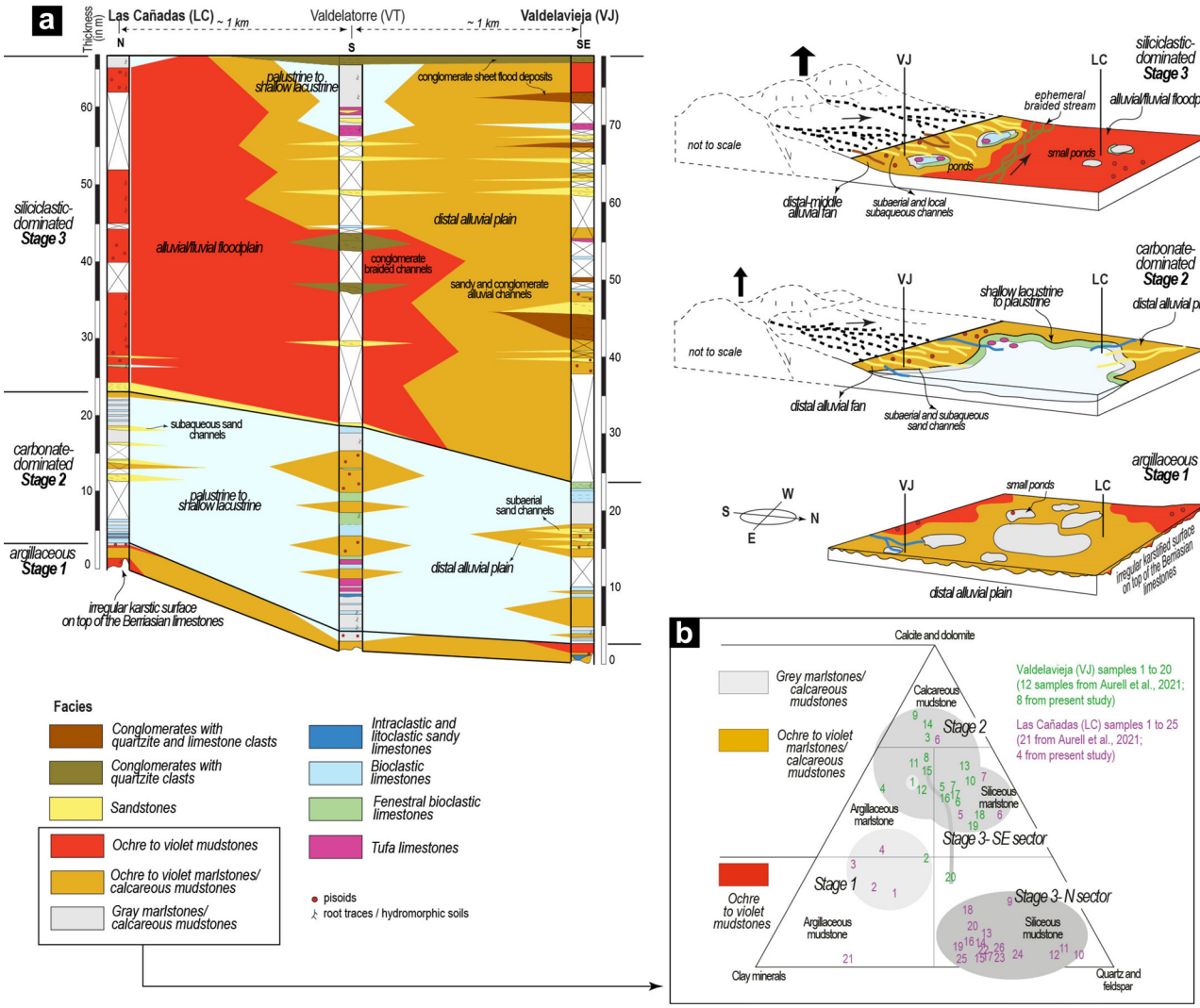

Fig. 2 **a** Facies correlation of the Torrelapaja Fm (SS-2) in the Bigornia Trough and sedimentary models of the three stages differentiated (adapted from Aurell et al., 2021). The detailed facies distribution recognized by Aurell et. al. (2021) in the Las Cañadas and Valdelavieja logs studied here is included in Fig. 5; **b** Mineralogical composition of muddy facies following the classification of Allix et. al. (2011)

based on the data collected in three logs (the LC, VT and VJ logs in Fig. 2a). The deposition of the muddy facies, limestones, sandstones, and conglomerates of this unit took place in distal alluvial fans and shallow lakes. The vertical and lateral distribution of facies allowed three sedimentary stages of evolution to be differentiated (Fig. 2a). The argillaceous Stage 1 corresponds to the sedimentary filling of the palaeokarstic surface on top of the underlying Ciria Fm (SS-1/SS-2 boundary) and is dominated by ochre to violet mudstones and ochre to violet mudstones/calcareous mudstones of argillaceous composition (Fig. 2b). The carbonate-dominated Stage 2 is characterized by the expansion of palustrine-lacustrine facies, localized alluvial clastic input (sandstones), and the deposition of carbonate-richer distal plain muddy facies (marlstone/calcareous mudstones; Fig. 2b). In the siliciclastic-dominated Stage 3, there is a significant increase in siliciclastic and a reduction in lacustrine-palustrine areas. Middle-distal alluvial fan channels (conglomerates with quartzite and limestone clasts, sandstones, and ochre to violet siliceous marlstones) developed southwards as a result of the increasing tectonic activity of this margin (Fig. 2a); by contrast, the northern area was dominated by an alluvial-fluvial plain with ochre to violet mudstones of siliceous composition and ephemeral braided streams (conglomerates with quartzite pebbles).

Of particular interest for the present study are the muddy facies recorded mainly in distal alluvial plains (Fig. 2b). The ochre to violet mudstones and ochre to violet marlstones/calcareous mudstones that accumulated in the distal alluvial plains have features indicating soil development (levels with Fe pisoids and root traces/hydromorphic horizons) and are similar to those found in lateritic palaeosols in age-equivalent units from the southern Maestrazgo Basin (Laita et al., 2020). The palustrine to shallow lacustrine grey marlstones/calcareous mudstones also contain Fe pisoids, which could be reworked from nearby distal alluvial plain areas (Aurell et al., 2021).

3 Samples and methods

The Las Cañadas (LC) and Valdelavieja (VJ) outcrops of the Torrelapaja Fm, previously studied by Aurell et. al. (2021) from a stratigraphic and sedimentological point of view, were selected for the sampling of the different muddy facies (Fig. 2b). They include ochre to violet mudstones, ochre to violet marlstones/calcareous mudstones, and grey marlstones/calcareous mudstones (hereinafter referred to as mudstones to calcareous mudstones), and some of them contain Fe pisoids (Fig. 3). On the whole, the VJ log represents deposition in a more proximal position of the distal alluvial plain compared to the LC log (Fig. 2a). A total of 49 samples (42 mudstone to calcareous mudstone samples and 7 Fe pisoids) were taken from throughout the two sections in order to analyse their texture and mineralogical composition (Table 1).

3.1 X-ray diffraction study

The 49 samples were studied by X-ray diffraction (XRD) to determine their mineralogical composition. The < 2 µm fractions were extracted by centrifugation and analysed in air-dried and ethylene–glycol-treated oriented aggregates to determine the clay minerals present in the samples.

To obtain the diffraction patterns, a Philips 1710 diffractometer was used at the University of Zaragoza (Zaragoza, Spain), with 40 kV voltage, 30 mA current, CuKα radiation, an automatic slit, and a graphite monochromator. The XRD patterns were acquired from 3 to 60 °C 2θ for the whole rock samples and from 3 to 30 °C for the < 2 µm fractions. In both cases, the goniometer velocity was 0.1º2θ/s and the integration time was 0.45 s. The recording was made with XPowderX software (Martin, 2017).

The relative proportions of the minerals were calculated using Reference Intensity Ratio (RIR) values from the literature (Biscaye, 1965; Schultz, 1964; Smith & Johnson, 2000). These RIR values were calculated in accordance with Hillier (2003). The kaolinite crystallinity (KC) was calculated measuring the full width at half maximum of the 001 reflection corresponding to 7 Å in the air-dried oriented aggregates. KC values are inversely related to kaolinite crystallinity, that is, the lower the KC value, the higher the kaolinite crystallinity.

3.2 Optical and electron microscopy study

To gain a precise mineralogical and textural characterization of the samples, seven thin sections of the mudstones to calcareous mudstones and Fe pisoids were selected for microscopy studies. Firstly, the thin sections were studied by transmitted and reflected light microscopy to identify both transparent and opaque minerals and to characterize their texture (Table 1). The seven thin sections and four rock fragments were then analysed using a Carl Zeiss Merlin field emission scanning electron microscope (FESEM) with an Oxford energy-dispersive X-ray (EDS) detector at the University of Zaragoza (Zaragoza, Spain) (Table 1). The thin sections had previously been carbon-coated. Compositional images were obtained using two detectors: an angular selective backscattered electron detector (AsB) and an energy selective backscattered electron detector (EsB). To obtain chemical information, semi-quantitative analyses were performed by energy-dispersive X-ray spectroscopy (EDS), with a detection limit of 0.1%. The accelerating voltage for the AsB and the EDS was 15 kV

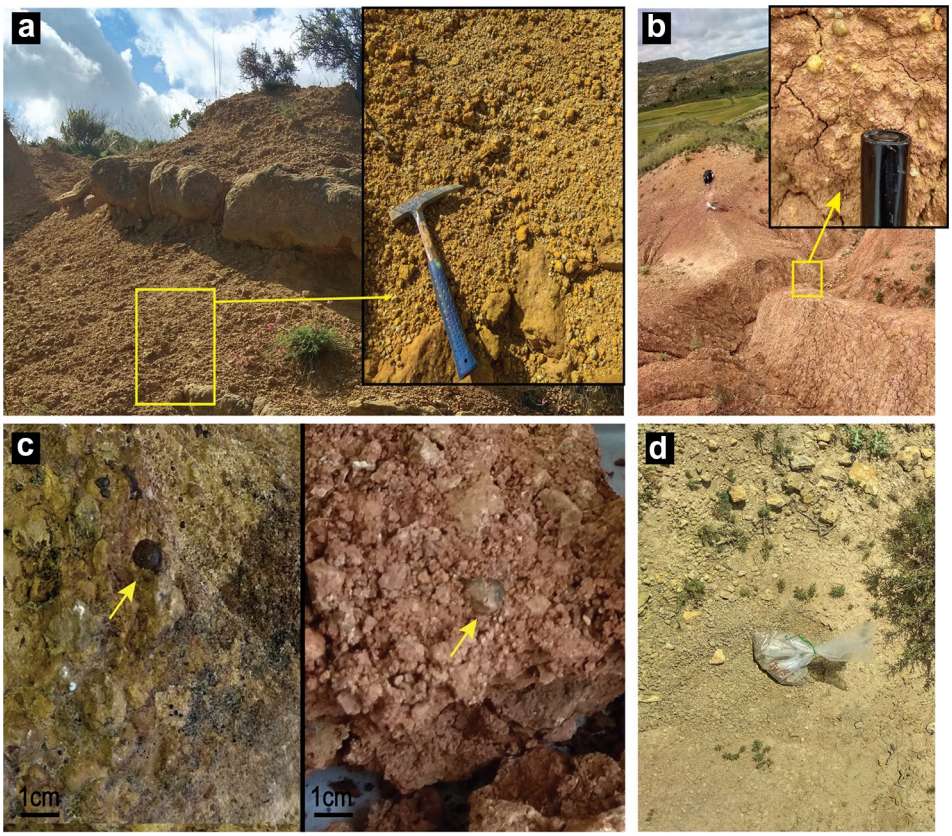

Fig. 3 **a** Close view of the VJ log showing ochre to violet mudstones interbedded with sandstones levels; **b** Close view of the LC log showing the ochre to violet mudstones; **c** Hand samples from the VJ (left) and LC (right) logs including Fe pisoids; **d** Close view of the VJ log showing the the grey marlstones/calcareous mudstones

with a beam current of 600 pA, whereas for the EsB, the accelerating voltage was 4 kV with a beam current of 1000 pA. Morphological images of the rock fragments were obtained using a secondary electron (SE) detector (in-lens) with an accelerating voltage of 5 kV and a beam current of 100 pA. In this case, the accelerating voltage was 5 kV with a beam current of 800 pA.

Table 1 Summary of sample analyses at the laboratory (n = number of samples/analyses)

Field samples (n = 49)	X-ray diffraction (Mineralogical composition)		Optical and electron microscopy (Textural and chemical analysis)	
	Whole rock (n = 49)	< 2 µm fraction of clays & clays/marls (n = 42)	Optical microscopy (n = 7)	Electron microscopy-FESEM/EDS (n = 11)
Ochre to violet clays/marls (n = 36)	36	36	5	9
Grey marls- (n = 6)	6	6	–	–
Ferruginous pisoids-7	7	–	2	2
	Relative proportions of the mineral phases	Clay minerals identification Kaolinite crystallinity	Textures Identification of opaque and transparent minerals	Micro- and nanotextures Chemical composition of the phases
	Derived data			

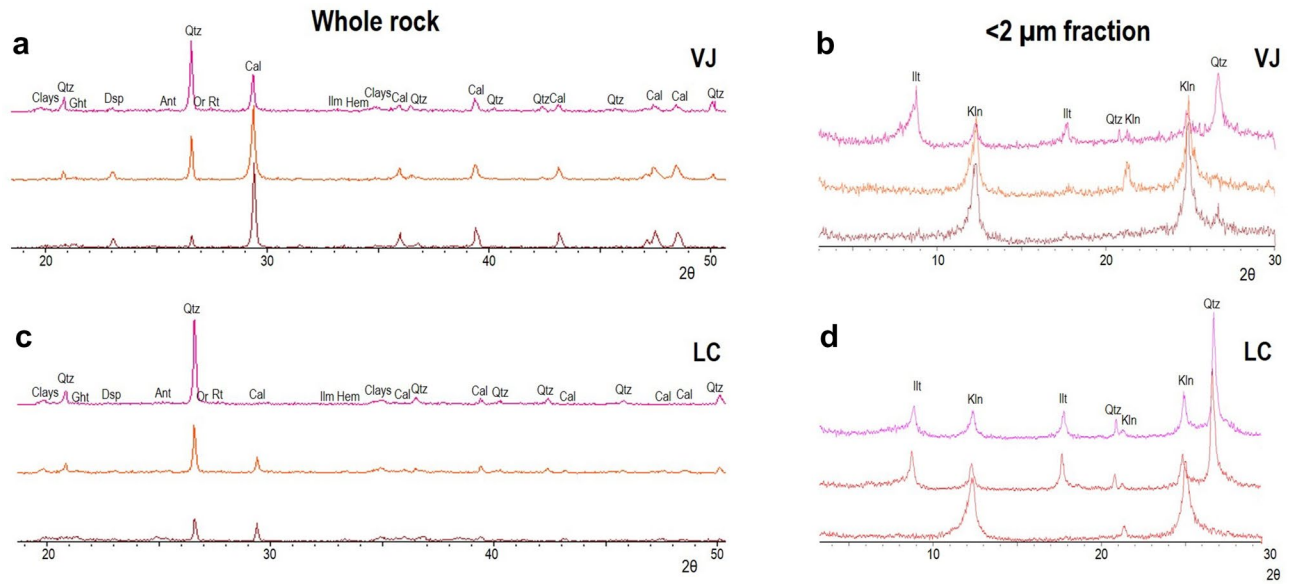

Fig. 4 XRD patterns obtained from the whole rock and < 2 µm fractions of samples in the VJ (**a** and **b**) and LC (**c** and **d**) logs. *Clays* = clay minerals, *Qtz* = quartz, *Cal* = calcite, *Dsp* = diaspore, *Ght* = goethite, *Ant*=anatase, *Or* = orthoclase, *Rt* = rutile, *Ilm* = ilmenite, *Hem* = hematite, *Kln* = kaolinite, *Ilt* = illitic phases

4 Results

4.1 Whole rock data

4.1.1 XRD data

The mudstones to calcareous mudstone of the LC and VJ logs are mainly formed by quartz, calcite, and clay minerals together with orthoclase, goethite, hematite, diaspore, anatase, rutile and ilmenite (Fig. 4). The XRD patterns of the whole rock show the same differences from bottom to top in both logs, with an increase in the intensity of quartz peaks and a decrease in those of calcite (Fig. 4a and c).

In the < 2 µm fraction, abundant kaolinite and illitic phases are identified in the XRD patterns (Fig. 4b and d). Characteristic reflections of kaolinite are observed at 7.14, 4.18, 3.84, 3.57 Å, and dickite and nacrite have not been detected. The term "illitic phases" includes both illite and micas (quantified together) as well as accessory random mixed-layer illite/smectite (I/S), which were identified in some of the < 2 µm fraction XRD patterns (but not quantified). These XRD patterns show a decrease in the intensity of kaolinite peaks to the top and that the illitic phases are detected from middle to top in both logs (Fig. 4b and d).

The whole rock mineralogical composition varies both vertically and laterally (Fig. 5a). On the whole, calcite is more abundant in the proximal VJ log (28–70%), whereas quartz + orthoclase predominate in the distal LC log (8–88%). In general, the calcite content decreases and quartz + orthoclase are more abundant towards the top of the logs. Clay minerals and goethite, hematite, diaspore, anatase, rutile, and ilmenite remain quite constant from the bottom to the top of the stratigraphic profiles. However, in detail there are slight vertical trends related to sedimentary stages 1 to 3. In the argillaceous Stage 1, the main lateral difference is the higher relative abundance of calcite in the proximal VJ log, and of clay minerals in the distal LC log. As regards the carbonate-dominated Stage 2, despite the presence of covered intervals (not sampled) in LC, a quite similar mineralogy dominated by calcite is recorded in both sections. The main lateral differences are recorded in the siliciclastic Stage 3, the proximal VJ log being dominated by calcite (with an upward decreasing trend), whereas in the distal LC log calcite is almost absent, especially at the top of the log, and quartz + orthoclase and clay minerals are more abundant compared to in VJ.

As regards the < 2 µm fraction, kaolinite is the main clay mineral in the lower mudstone to calcareous mudstone levels (> 50%), but its content decreases upwards coeval with an increase in the content of illitic phases. More specifically, samples of the argillaceous Stage 1 are only formed by kaolinite in the proximal VJ log but also have illitic phases in the distal LC log. In the carbonate-dominated Stage 2, kaolinite is again the main clay in the proximal VJ log, whereas in the distal LC log illitic phases predominate. This predominance of illitic phases is observed in both sections in the siliciclastic-dominated Stage 3, with a particularly notable upward increase in the proximal VJ log.

Kaolinite crystallinity is shown in Fig. 5b and in Table 2. In the argillaceous Stage 1, in the distal LC log (with its

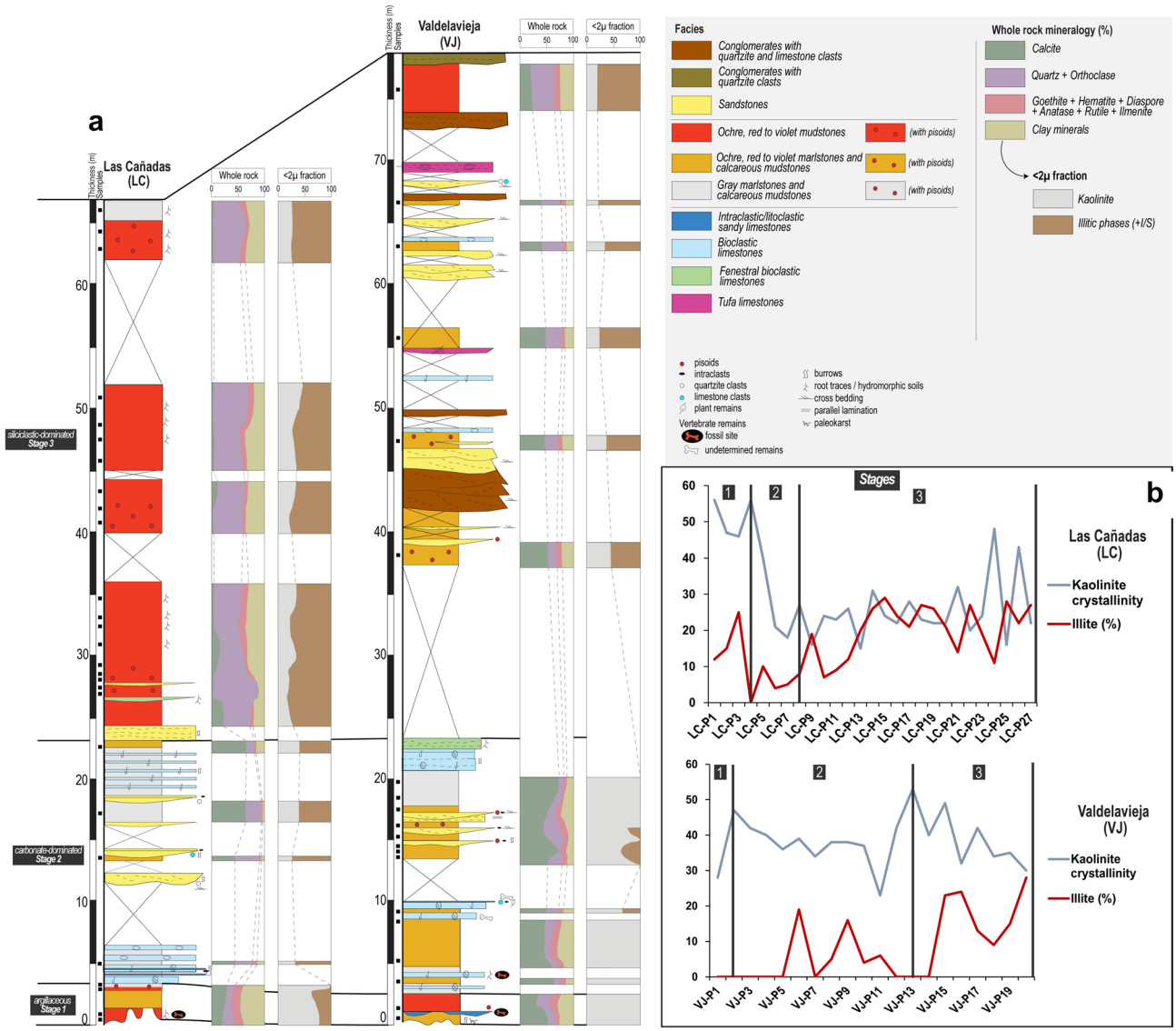

Fig. 5 **a** Variations in mineral content of the mudstones to calcareous mudstones in the LC and VJ logs; **b** Evolution of kaolinite crystallinity vs content of illitic phases from bottom to top of the logs. The kaolinite crystallinity value was multiplied by 100 for comparison with the content of illitic phases. Lower values indicate higher kaolinite crystallinity, and vice versa

higher relative proportion of clay minerals including a predominance of kaolinite over illitic phases), kaolinite is less crystalline than in the proximal VJ log, where kaolinite is the only clay mineral and there is a higher relative abundance of calcite. In the carbonate-dominated Stage 2, with calcite predominating in both sections, kaolinite is slightly less crystalline and predominates in the proximal VJ log, whereas in the distal LC log, where illite predominates, an increase in kaolinite crystallinity can be observed upwards. In the siliciclastic Stage 3, in the proximal VJ log, kaolinite crystallinity shows an increasing trend coupled with an increase in illitic phases and a decrease in calcite. By contrast, in the distal LC log, dominated by quartz + orthoclase and clay minerals (illitic phases), the kaolinite crystallinity is higher compared to the previous Stages 1 and 2, but decreases in some samples towards the top of the log, where the content of illitic phases is somewhat lower. Although there is not a general trend in kaolinite crystallinity, it should be noted that during Stage 3, especially in the distal LC log, kaolinite is more crystalline when the proportions of illitic phases are higher.

4.1.2 Optical and electron microscopy data

The optical microscopy images show that the mudstones to calcareous mudstones are formed by a fine-grained matrix composed of clay minerals and oxides that cannot be identified at optical microscope resolution (Fig. 6a–b). Abundant quartz clasts (40–200 μm) are recognised (Fig. 6a).

Table 2 Kaolinite crystallinity values of the samples of mudstones to calcareous mudstones measured in air-dried (AD) samples

Valdelavieja (VJ)			Las Cañadas (LC)		
Sample number	Muddy facies	KC Air-dried (001)	Sample number	Muddy facies	KC Air-dried (001)
1	OVMC	0.28	1	OVM	0.56
2	OVM	0.47	2	OVM	0.47
3	GMC	0.42	3	OVM	0.46
4	OVMC	0.40	4	GMC	0.56
5	OVMC	0.36	5	GMC	0.40
6	OVMC	0.39	6	OVMC	0.21
7	OVMC	0.34	7	GMC	0.18
8	OVMC	0.38	8	GMC	0.16
9	OVMC	0.38	9	OVM	0.16
10	OVMC	0.37	10	OVM	0.24
11	OVMC	0.23	11	OVM	0.23
12	OVMC	0.42	12	OVM	0.26
13	GMC	0.53	13	OVM	0.15
14	GMC	0.40	14	OVM	0.31
15	OVMC	0.49	15	OVM	0.24
16	OVMC	0.32	16	OVM	0.22
17	OVMC	0.42	17	OVM	0.28
18	OVMC	0.34	18	OVM	0.23
19	OVMC	0.35	19	OVM	0.22
20	OVM	0.30	20	OVM	0.22
			21	OVM	0.32
			22	OVM	0.20
			23	OVM	0.24
			24	OVM	0.48
			25	OVM	0.16
			26	OVM	0.43
			27	GMC	0.22

Classification of muddy facies from Aurell et. al. (2021)

OVM=ochre to violet mudstones, *OVMC*=ochre to violet marlstones/calcareous mudstones, *GMC*=grey marlstones/calcareous mudstones

Microsparitic carbonate nodules (100 µm to 1 mm in size; Fig. 6b), as well as microsparitic calcite filling pores in the matrix, are also present.

Compositional (EsB and AsB) and secondary electron (SE) images of the lower mudstone to calcareous mudstone levels show that kaolinite appears in the matrix both as subhedral to euhedral nanometric plates, commonly showing pseudohexagonal outlines with random orientation (Fig. 6c and d), and as booklets 1–10 µm in length (Fig. 6e–f).

In samples where illitic phases predominate (towards the upper mudstone to calcareous mudstone levels), smectite flakes (not detected by XRD) are also observed (Fig. 7a). The illitic phases are heterometric (1–10 µm) and present wavy and anhedral morphologies and frequently separated sheets (Fig. 7a–c). Intergrowths of illitic phases and kaolinite are also observed (Fig. 7c), like those described in similar materials (Bauluz et al., 2014; Do Campo et al., 2018).

According to the optical microscopy study, the carbonate both in the nodules and filling pores in the matrix is sparitic and/or microsparitic, and the EDS analyses indicate calcite compositions (Fig. 7d and e). Occasionally, some of the carbonate nodules are cemented by kaolinite (Fig. 7e). Fibrous calcite crystals cementing the matrix are also present (Fig. 7f).

EDS average analyses of the kaolinite, illitic phases, and smectite, as well as the average chemical formulae calculated, are included in Table 3. According to these analyses, the kaolinite composition is close to the theoretical one but presents low proportions of Fe ($\leq$0.1 a.p.f.u.). The illitic phases compositions are within the range commonly reported in the bibliography. The smectite compositions correspond to dioctahedral smectite, given the higher content of trivalent cations (Al and Fe) in the octahedral layer, and are consistent with a montmorillonite-type smectite.

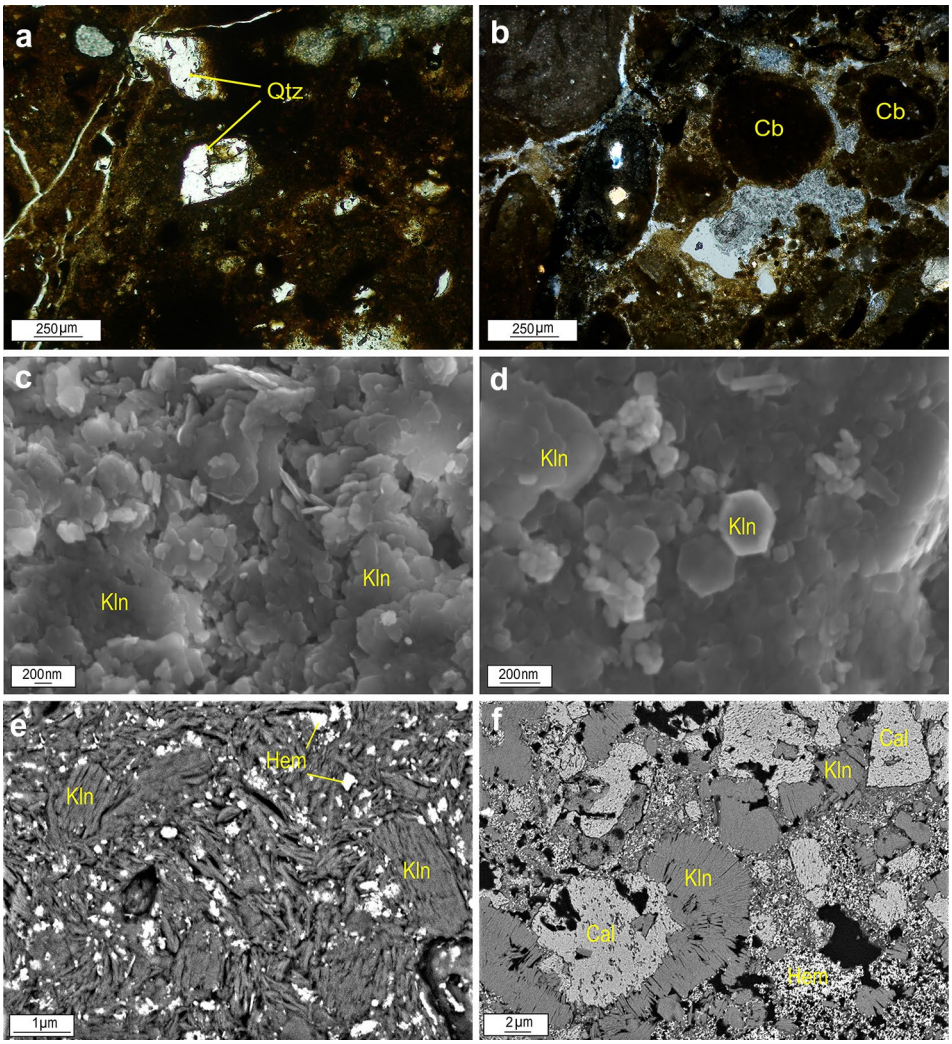

Fig. 6 Transmitted light optical microscopy images (**a** and **b**) and SEM images (**c**–**f**) of the lower mudstone to calcareous mudstone levels. **a** Quartz clasts in the matrix of the mudstones to calcareous mudstones from the LC log; **b** Microsparitic carbonate nodules in the mudstones to calcareous mudstones from the VJ log; **c** and **d** SE images showing platy kaolinite aggregates with random orientation and pseudohexagonal outlines; **e** 1–2 µm-sized kaolinite booklets and hematite crystals; **f** Kaolinite booklets reaching up to 10 µm in length and growing on microsparitic calcite nodules. *Qtz* = quartz, *Cb* = carbonate, *Kln* = kaolinite, *Hem* = hematite, *Cal* = calcite

4.2 Pisoid data

The Fe pisoids are embedded in the clay-rich matrix of the mudstone to calcareous mudstones. They are from 3 mm to 1 cm in diameter and show spherical to ellipsoidal morphologies and some of them are fractured. According to their size, following the classification given by Bárdossy (1982): macropisoids (> 5 mm), pisoids (1–5 mm), ooids (100–1000 µm) and micro-ooids (< 100 µm), the Fe pisoids are pisoids and macropisoids.

On the other hand, Reolid et. al. (2008) also classified as ferruginous ooids and pisoids those grains formed by a nucleus enveloped by an iron oxide coating, which also fits with the Fe pisoids of this study. According to their morphological features and lamination, these pisoids and macropisoid would be included in the Type A ooids and pisoids defined by these authors, which are formed by a thin, regular lamination that forms concentric layers enclosing a nucleus. In Type A ooids and pisoids, the nucleus can be a fragment of an older ferruginous ooid or an indeterminate ferruginous lump. The nuclei of the Fe pisoids studied here are always formed by and indeterminate ferruginous lump, so following the classification given by Guerrak (1987) they can also be classified as simple pisoids.

4.2.1 XRD data

The XRD patterns of two macropisoids (one of each log) indicate that they contain quartz, clay minerals, hematite, goethite, together with orthoclase, diaspore, anatase, rutile, and ilmenite (Fig. 8a). Calcite was also detected in the XRD patterns (especially in those of the macropisoids from the LC log), but it is not represented because, as it will be explained below, part of this calcite was not formed coetaneously with the mudstones and calcareous mudstones and the Fe pisoids. The relative proportions of these phases indicate that the macropisoids from the two logs are mainly formed by quartz, clay minerals (kaolinite and illitic phases, as deduced from the FESEM results), hematite, goethite and minor amounts of orthoclase, diaspore, anatase, rutile and ilmenite (Fig. 8b).

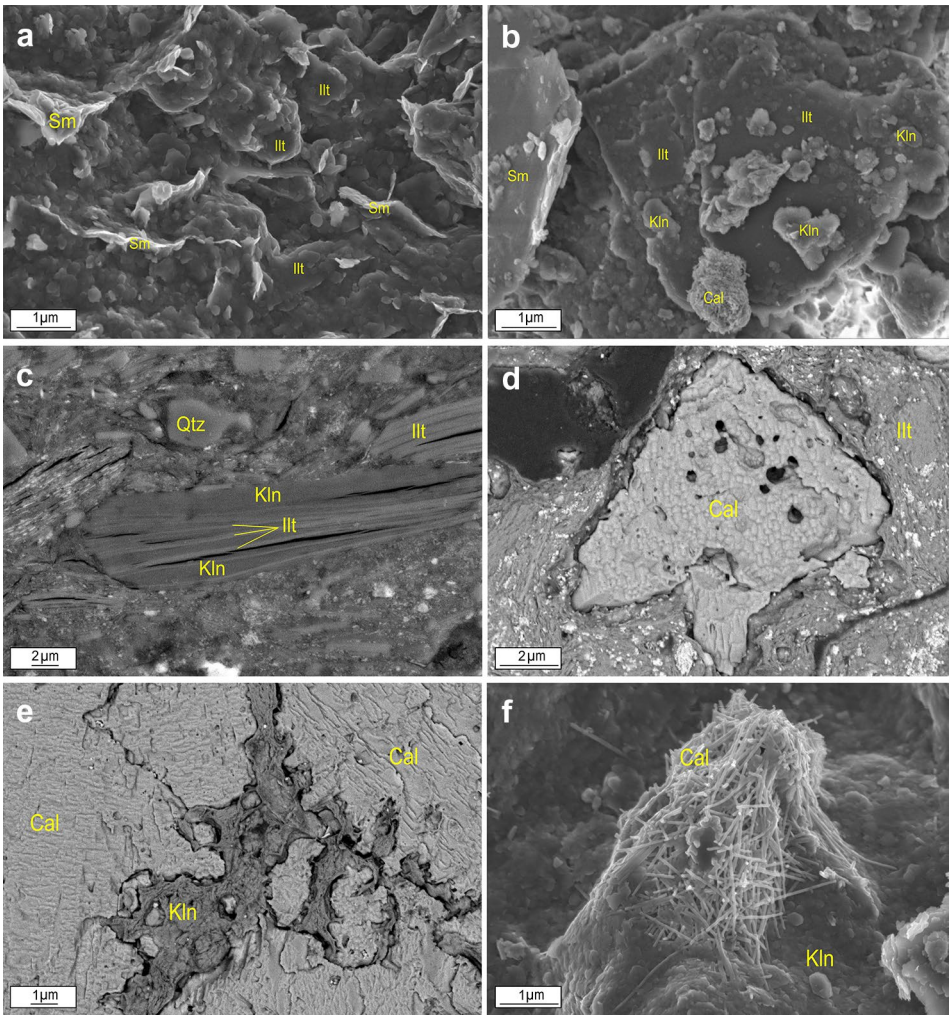

Fig. 7 FESEM images of the matrix of the middle and upper mudstones to calcareous mudstones (**a**–**c**) and the carbonates observed in the mudstones to calcareous mudstones (**d**–**f**). **a** SE image of smectite flakes and anhedral illitic phases; **b** SE image of anhedral illitic phases and subhedral kaolinite; **c** BSE images showing intergrowths of illitic phases and kaolinite; **d** Microsparitic calcite filling a matrix pore; **e** Kaolinite cementing calcite in a microsparitic nodule; **f** Fibrous calcite crystals cementing the matrix of the mudstone to calcareous mudstone. *Sm* = smectite, *Kln* = kaolinite, *Ilt* = illitic phases, *Qtz* = quartz, *Cal* = calcite

Table 3 EDS analyses (Wt%) of clay minerals in the mudstones and calcareous mudstones (standard deviation in brackets)

	O	Na	Mg	Al	Si	K	Ti	Fe	Calculated formula
Kaolinite ($n=28$)	49.08 (2.83)	–	–	21.88 (1.20)	24.87 (1.46)	–	0.21 (0.31)	3.95 (3.56)	$Fe_{0.1}Al_{1.9}Si_2O_5(OH)_4$
Illitic phases ($n=33$)	45.72 (2.12)	0.16 (0.26)	0.68 (0.36)	16.75 (3.20)	26.21 (2.84)	8.23 (2.23)	0.08 (0.20)	2.18 (1.44)	$(K_{0.8},H_3O)(Al_{1.7}Mg_{0.1}Fe_{0.2})(Si_{3.4}Al_{0.6})O_{10}[(OH)_2,(H2O)]$
Smectite ($n=20$)	44.90 (3.20)	0.14 (0.21)	1.42 (2.95)	18.38 (2.92)	25.64 (5.13)	4.94 (1.34)	0.39 (0.98)	4.22 (3.36)	$(K_{0.5})(Al_{1.7}Fe_{0.3}Mg_{0.1})(Si_{3.3}Al_{0.7})O_{10}(OH)_2nH_2O$

4.2.2 Optical and electron microscopy data

The pisoids and macropisoids are constituted by a nucleus and an outer cortex formed by several layers, both composed of a mixture of hematite, goethite, and clay minerals (Fig. 9a–c). In the case of the macropisoids, the outer cortex is 1–3 mm thick, and quartz clasts are frequently included among the layers (Fig. 9b and c). The nucleus is formed by an indeterminate ferruginous lump along with goethite and hematite. Both hematite and goethite show botryoidal textures, occasionally in alternating layers (10–30 µm) and some parts of the nucleus are replaced by carbonate at times (Fig. 9d). The electron microscopy images show that the

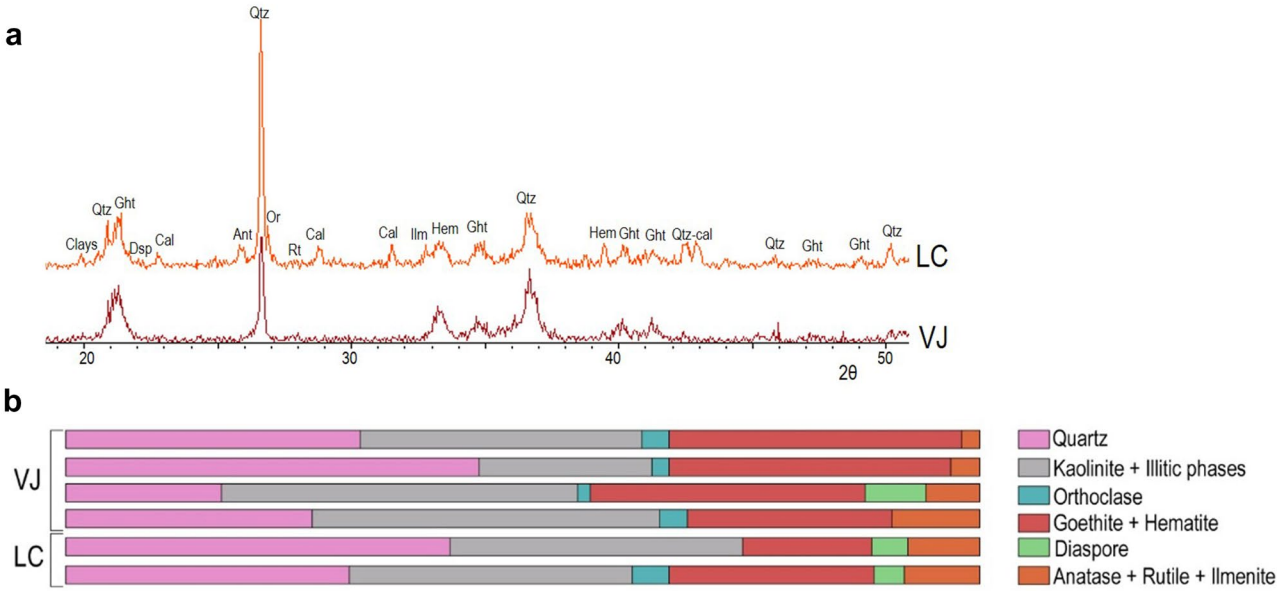

Fig. 8 **a** XRD patterns of two macropisoids from the VJ and LC logs; **b** relative proportions of mineral phases in several macropisoids from the LC and VJ logs

layers constituting the cortex of the macropisoids are formed by different amounts of kaolinite mixed with hematite and goethite, allowing one layer to be differentiated from another based on its kaolinite content. Hematite frequently cements kaolinite in the macropisoids (Fig. 9e). In both the pisoids and macropisoids, there is kaolinite with platy shapes with random orientation and as booklets like those found in the matrix of the lower mudstone to calcareous mudstone levels (Fig. 9e). Intergrowths of illitic phases and kaolinite with the same morphologies as those found in the upper mudstone to calcareous mudstone levels are also observed (Fig. 9f). Microsparitic calcite and occasional barite fill cavities in the macropisoids (Fig. 9f and g).

5 Discussion

5.1 Origin of the clay minerals, pisoids, and carbonates in the palaeosols

The mineralogy of the mudstone to calcareous mudstone levels consists of calcite, quartz (and orthoclase), clay minerals (kaolinite, illitic phases, smectite), Fe and Ti oxides, and Fe oxyhydroxides. The high content in clay minerals, along with the oxides and oxyhydroxides and the presence of Fe pisoids is a consequence of the development of palaeosols in the Torrelapaja Fm. The determined mineralogical association is common in oxisols, as categorised by the Soil Taxonomy Classification.

Compositional and morphological images show that the platy kaolinite is commonly euhedral to subhedral and displays pseudohexagonal outlines, indicating that it is probably authigenic. The presence of kaolinite booklets is not compatible with a detrital origin since they are too delicate to withstand erosion or transport processes, thus suggesting that they formed in-situ during the edaphic process (Bauluz et al., 2014; Do Campo et al., 2018; Laita et al., 2020). The lower and variable relative crystallinity of kaolinite in Stages 1 and 2 could be attributed to the presence of Fe in the kaolinite structure (as detected in EDS analyses, although in low proportions), since substitutions of Al by Fe in the octahedral sheet of kaolinite has been described in similar materials (Laita et al., 2020; Mendelovici et al., 1979) and is something common in weathering processes (Cantinolle et al., 1984; Mestdagh et al., 1980; Yuste et al., 2015). On the other hand, the kaolinite presents somewhat higher crystallinity towards the top of the studied logs, coeval with the increase in illitic phases in Stage 3 and the presence of intergrowths of illitic phases and kaolinite, in which the illitic phases act as a substrate for the kaolinite crystallization. This may enhance more effective crystallization of kaolinite.

Smectite is detected by electron microscopy but not by XRD, probably because its content lies below the detection limit of XRD. The flake-type morphologies observed in the smectite by electron microscopy suggest an in-situ origin, and the EDS analysis indicates that it corresponds to dioctahedral montmorillonite-type smectite. This kind of smectite has previously been reported in palaeosols as a product of the weathering of feldspars and micas (Fesharaki et al.,

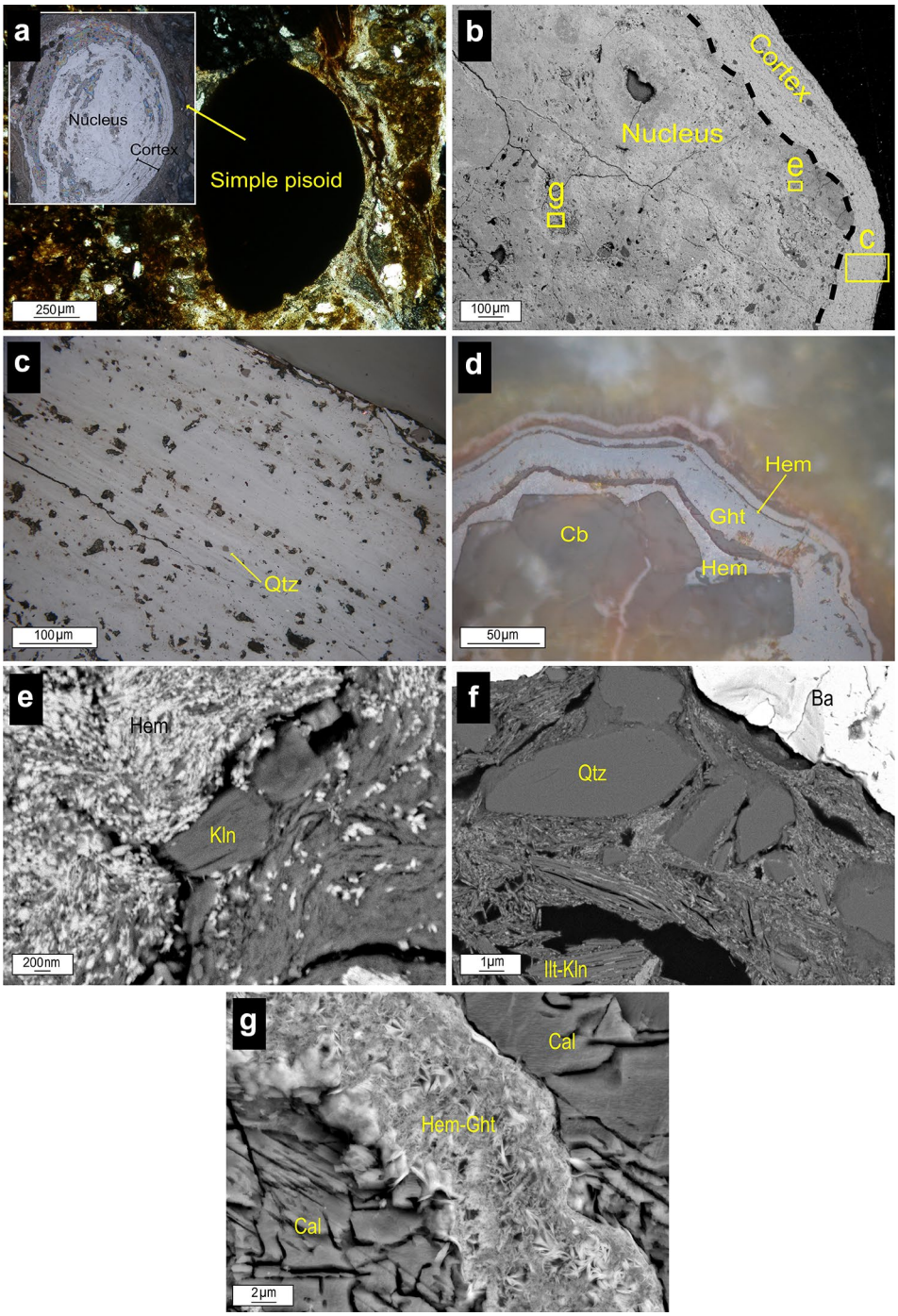

Fig. 9 Transmitted and reflected light optical microscopy and SEM images of pisoids and macropisoids. **a** Simple pisoid from the LC log; **b** Nucleus and cortex of a macropisoids. The squares show the areas were the enlarged images **c**, **e** and **g** were taken; **c** Macropisoid cortex formed by several layers with quartz clasts included among the layers; **d** Hematite and goethite forming alternating layers in the nucleus of a macropisoids and microsparitic carbonate replacing partially the nucelus; **e** Booklets of platy kaolinite and hematite in the nucleus of a macropisoid; **f** Quartz clasts, barite filling cavities, and illitic phases/kaolinite intergrowths in the nucleus of a macropisoid; **g** Microsparitic calcite filling cavities of a macropisoid. *Qtz* = quartz, *Cb* = carbonate, *Hem* = hematite, *Ght* = goethite, *Kln* = kaolinite, *Ilt* = illitic phases, *Ba* = barite, *Cal* = calcite

2007). Kaolinite and smectite would have thus been formed during the edaphic process by the dissolution of previous aluminium silicates (e.g., feldspars and illitic phases).

Authigenic illite is described in brackish and freshwater clays, lacustrine marls and gleysols during the Eocene–Oligocene, due to illitization of smectite and mixed-layer I/S during pedogenic processes (Huggett & Cuadros, 2005, 2010; Huggett et al., 2001). However this process is not observed in the uppermost Hauterivian–lower Barremian palaeosols studied here, which can be classified as oxisols. The origin of illitic phases in palaeosols is not compatible with the genesis of kaolinite (Bauluz et al., 2000). Detrital illite can degrade to interstratified illite–smectite under humid conditions (Chamley, 1989). Smectitization of illite induced by pedogensis has also been described in palaeosols (Meenakshi et al., 2020; Schaetzl & Thompson, 2015). The fact that the illitic phases studied here act as a substrate for kaolinite crystallization indicates that they are former phases

(Bauluz et al., 2014). Thus, these illitic phases may have a detrital origin and intervene in the genesis of kaolinite and smectite during the edaphic process. In addition, their anhedral morphologies are consistent with a detrital origin (Bauluz et al., 2014; Laita et al., 2020).

The calcite nodules observed in some of the mudstone to calcareous mudstone levels are cemented by kaolinite, pointing to a previous genesis for the nodules. Other investigations (Laita et al., 2020; Mücke et al., 1999) suggest that soil development usually occurs in various episodes involving changes in the water level and reworking processes. In the present study, the calcite nodules may come from the underlying limestone levels generated during the rising of the water level. A subsequent lowering of the water level would allow the calcite nodules to be cemented by kaolinite. This would also be the factor responsible for the reworking and fracturing of some of the macropisoids.

As other authors suggest (Rossi & Cañaveras, 1999), the fibrous calcite crystals cementing the matrix of the mudstone to calcareous mudstone levels would have formed during diagenesis. This diagenesis would also allow the filling of the matrix pores and macropisoids cavities and the replacements of some parts of their nuclei by microsparitic calcite. The barite observed within the cavities of macropisoids may also have a diagenetic origin; it has been described cementing palaeosols in other areas (Michel et al., 2016). The calcite and barite cements thus postdate the kaolinite and smectite. These cements must have therefore formed during early diagenesis, which would not have altered the palaeoclimatic signal registered in the clay minerals formed in-situ.

Saber et. al. (2018) classified ferriferous pisoids formed by in-situ growth in lateritic weathering profiles according to their mineralogical composition as: (1) pure kaolinitic pisoids, (2) kaolinitic-hematitic or hematitic-kaolinitic pisoids, and (3) hematitic pisoids. The second group includes those pisoids whose inner nucleus is composed of kaolinite and/or hematite surrounded by an outer cortex formed by kaolinite and hematite laminae. This latter subgroup is consistent with the pisoids and macropisoids studied here, since according to the XRD and electron microscopy results, they are mainly formed by hematite, goethite, kaolinite, and occasional quartz and illitic phases. FESEM images indicate that the kaolinite in the macropisoids displays platy morphologies and also occurs as booklets, similar to the kaolinite found in the matrix constituting the lower mudstone to calcareous mudstone levels. Likewise, the illitic phases and the intergrowths of illitic phases and kaolinite in the macropisoids are similar to those observed in the matrix of the upper mudstone to calcareous mudstone levels.

According to Bárdossy (1982), the formation of Fe pisoids and macropisoids in soils is usually associated with conditions of permanent groundwater saturation. These conditions are congruent with the genesis of Type A ferruginous ooids and pisoids described by Reolid et. al. (2008). The growth of the concentric layers that form the cortex of the pisoids and macropisoids also indicates physical and chemical changes in the environmental conditions, giving place to the precipitation of several mineral phases, such as kaolinite and Fe and Ti oxides, and Fe oxyhydroxides, in different quantitates (Yuste et al., 2020).

These data, along with the concentric structure and morphology of the Fe pisoids studied here indicate that they would have an in-situ origin and were thus formed during the edaphic process. However, the fractures observed in the macropisoids filled with calcite and barite also suggest that they underwent some reworking. On the other hand, the presence of hematite cementing kaolinite in the macropisoids indicates that the genesis of Fe oxides took place during the edaphic process but after the formation of kaolinite, as described in similar materials in the Iberian Range (Laita et al., 2020).

5.2 Clay mineral trends and climate vs. tectonic controls

5.2.1 Clay minerals and sediment supply

The clay minerals show vertical and lateral trends related to the three sedimentary stages defined by Aurell et. al. (2021), which can shed some light on the factors (climate, tectonics) controlling the genesis of the mineralogical assemblages and the development of the palaeosols.

Stage 1 is dominated by distal alluvial plain muddy facies of argillaceous composition (Fig. 2), with a somewhat lower quartz content and higher clay mineral content in the distal LC log (kaolinite being the main clay mineral) but higher calcite content in the proximal VJ log. This lateral trend could be associated with local factors (e.g., differential supply) but the reduced sediment thickness of this stage and lack of significant sedimentological differences between the logs precludes a more definitive interpretation (Figs. 2 and 5). Stage 2 is characterised by an increase in the water level, allowing the expansion of palustrine-lacustrine areas, but also a coeval increase in the terrigenous sediment supply (Aurell et al., 2021; Fig. 2). The mineralogical composition of distal alluvial plain and palustrine muddy facies is very homogeneous, as they are dominated by calcite in the distal LC and proximal VJ logs. In addition, kaolinite predominates over illitic phases in the proximal VJ log, as in Stage 1. These data reflect the fact that there is no significant control of the increasing terrigenous supply in the soil development during this stage. Stage 3 is characterised by an increase in terrigenous-clastic supply due to an increase in tectonic activity in southern areas (VJ log; Fig. 2) (Aurell et al., 2021). The change in the sedimentological conditions during this stage, with a greater contribution of terrigenous

sediment, leads to higher amounts of quartz and illitic phases (Fig. 5). Nevertheless, calcite, with a decreasing tendency, is present in the proximal VJ log, where a greater terrigenous supply is recorded. As explained below, the higher crystallinity of kaolinite towards the top of the logs may be a consequence of the higher quantities of illitic phases. These illitic phases form intergrowths in which they act as a substrate for the growth of the kaolinite, enhancing a more effective crystallization for the kaolinite. Additionally, the increase in quartz content towards the top of the profiles, may generate a possible increase in the porosity of the upper mudstone to calcareous mudstone levels, which could allow the kaolinite to be more crystalline and also favour the genesis of calcite cements during diagenesis as it would lead to better conditions for fluid circulation.

5.2.2 Clay minerals and palaeoclimate

As commented in a previous section, the mineralogical association determined in the mudstone to calcareous mudstone levels of this research is common in oxisols, as categorised by the Soil Taxonomy Classification. Oxisol development occurs under humid tropical climates (Do Campo et al., 2018).

Several authors have reported mineral assemblages comprising goethite, hematite, aluminium hydroxides, kaolinite, and quartz, as well as the presence of Fe pisoids in lateritic palaeosols (e.g., Bauluz et al., 2014; Giovannini et al., 2017; Nkalih Mefire et al., 2018; Nouazi Momo et al., 2019; Yuste et al., 2017).

On the other hand, the genesis of the palaeosols in the Torrelapaja Fm was also coeval with a rise and possibly a subsequent fall in the water level, as evidenced by the presence of kaolinite cementing calcite nodules and of reworked features in the pisoids.

The general climate described for the Hauterivian–Aptian period in Western Europe includes a trend from seasonal to warm climates and then to cooler conditions. During the Hauterivian, a seasonal climate prevailed (Föllmi, 2012; Godet et al., 2008), evidenced by the presence of illite and smectite in marine sedimentary successions (Mutterlose & Ruffell, 1999). From the latest Hauterivian to early Barremian, the increase in kaolinite in the palaeosols is consistent with a trend towards warmer conditions (Bárdossy, 1982; Föllmi, 2012; Godet et al., 2008; Wright et al., 2000), which prevailed during the mid and late Barremian (Scotese et al., 2021). On the other hand, during this period, Moiroud et. al. (2012) also reported marl–limestone alternations, with limestones enriched in I/S mixed-layers and kaolinite and illite-rich marls. According to these authors, the presence of kaolinite and illite in the marls is a consequence of continental runoff under humid tropical conditions, whereas the I/S contained in the limestones were formed under seasonally semi-arid conditions. Thus, this is reflecting a distortion in the climatic signal obtained from the clay minerals assemblages formed in continental or marine domains. A later change from warm to cooler conditions is recorded during the early Aptian (Dinis et al., 2020; Godet et al., 2006; Steuber et al., 2005).

As pointed out by Laita et. al. (2020), the trend in humidity during the Early Cretaceous of Western Europe is not so clear. Clay mineral assemblages from French and Swiss sections show a change from dry to more humid conditions during the Hauterivian (Godet et al., 2008). In the Tethys area, arid and humid regimes are recorded during the late Hauterivian (Föllmi, 2012), and temperature models show warm and humid conditions for the early Barremian (Bodin et al., 2009; Föllmi, 2012; Price et al., 2011). However, alternate wet and dry seasons during the early Barremian have also been reported (Haywood et al., 2004). Finally, an increase in humid conditions is described during the mid-Barremian in Europe (Mutterlose et al., 2014), whereas $\delta^{18}O$ records show a trend towards cooler and more arid conditions towards the late Barremian of the Tethys (Föllmi, 2012).

In northwestern Spain, a seasonal subtropical climate is described during the Early Cretaceous (Buscalioni & Fregenal-Martínez, 2010). In addition, the presence of Barremian kaolinite-rich bauxites and laterites in the Iberian Range (NE Spain) is also consistent with warm and humid conditions (Bauluz et al., 2014; Laita et al., 2020; Yuste et al., 2015, 2017).

In the western part of the Cameros Basin, stacked sheet flood deposits and sandy channels, along with conglomerates, mottled mudstones, and pedogenic carbonates included in the Piedrahita de Muñó Formation (Barremian–Aptian), suggest a semi-arid climate with seasonal rainfall (Platt, 1989).

In the uppermost Hauterivian–lower Barremian Torrelapaja Fm of the Torrelapaja subbasin (southeastern Cameros Basin), XRD and electron microscopy results show a higher content of kaolinite formed in-situ in the lower mudstone to calcareous mudstone levels, suggesting an intense chemical weathering characteristic of a warm and humid climate (Bauluz et al., 2014; Nouazi Momo et al., 2019; Raucskik & Varga, 2008; Won et al., 2018). As regards the pisoids and macropisoids, these would have been formed in environments of permanent groundwater saturation, which would have occurred in different episodes during the three sedimentary stages.

The decrease in kaolinite towards the top of the stratigraphic profiles correlates with the increase in the content of detrital quartz and illitic phases, which is related to a greater terrigenous-clastic supply during Stage 3. This could have partially inhibited soil formation. On the other hand, this trend is also coeval with the presence of authigenic smectite,

thus reflecting a decrease in chemical weathering perhaps associated with a change to colder and drier conditions during the late Hauterivian–early Barremian in this part of the Cameros Basin. In addition, the above-mentioned alternating goethite-hematite sequences in the macropisoids are also associated with less humid conditions (Laita et al., 2020; Velasco et al., 2013).

In the east of the Maestrazgo Basin (SE Iberian Range), the presence of laterites in the Cantaperdius Formation (Barremian–Aptian) has been reported (Combes, 1990; Salas, 1987). In the nearby Morella subbasin, karst bauxite deposits, which probably developed from lateritic materials laterally equivalent to the Cantaperdius Fm, have also been described (Molina & Salas, 1993; Yuste et al., 2015). Moreover, in the Oliete subbasin (NW Maestrazgo Basin), Laita et. al. (2020) described a decrease in kaolinite and an increase in smectite and illite content in lateritic palaeosols present in the lower part of the Blesa Formation (early Barremian), which reflected a change from warm/humid to cold/dry conditions. The lateritic palaeosols described in the lower Blesa Fm are regarded as age-equivalent with the palaeosols from Stages 1 and 2 of the uppermost Hauterivian–lower Barremian Torrelapaja Fm (Aurell et al., 2021). The same tendency in the climatic conditions can be deduced in this part of the Cameros Basin, but the record is not as good as in the Oliete subbasin due to the high siliciclastic contribution during Stage 3, associated with an increase in tectonic activity. All these data reflect warm and humid conditions during the early Barremian in these two Iberian subbasins over 100 km apart, followed by a change to drier, colder conditions, at least in the Oliete subbasin (Maestrazgo Basin, SE Iberian Range; Laita et al., 2020), which could also have taken place in the Torrelapaja subbasin (Cameros Basin, NW Iberian Range).

6 Conclusions

A combination of facies analysis and a study of the clay mineralogy of clay/marl-rich outcrops has allowed us to characterize the mineralogical and textural changes found in the mudstones to calcareous mudstones of the Torrelapaja Formation (uppermost Hauterivian–lower Barremian).

Kaolinite is the main clay mineral in the lower levels. Its euhedral morphologies and the presence of aggregates forming booklets indicate an authigenic origin for this mineral. The growth of the kaolinite to form intergrowths with illitic phases indicates that the illitic phases are former phases and act as a substrate for the kaolinite crystallization. This may favour the higher crystallinity of kaolinite in the upper levels, whereas the lower Fe proportions in the kaolinite in the lower levels could be the reason for its lower crystallinity. The smectite (montmorillonite-type composition) detected in the upper levels and its flake-type morphologies are consistent with an authigenic origin. The mineralogy and structure of the pisoids and macropisoids also reflect an in-situ origin during the edaphic process, but some of them are fractured, indicating reworking processes.

The matrix of the mudstones to calcareous mudstones and the cavities of the pisoids were later cemented by microsparitic calcite (and barite in some macropisoids) during early diagenesis. This diagenesis did not alter the palaeoclimatic signal registered in the kaolinite and smectite formed in-situ.

The mineralogical association in the mudstones and calcareous mudstones is characteristic of oxisols (laterites), which developed under humid tropical climates.

The higher content of kaolinite formed in-situ in the lower levels suggests intense chemical weathering as a consequence of a warm and humid climate, which is consistent with the palaeoclimatic conditions reported during the latest Hauterivian–early Barremian in the NE of the Iberian Plate.

The decrease in the kaolinite content, along with the increase in quartz and illitic phases, in the upper levels is related with an increase in siliciclastic input during Stage 3, which may have inhibited soil genesis. However, this trend in kaolinite content, along with the presence of authigenic smectite, also reflects a decrease in chemical weathering, perhaps associated with a change to colder and drier conditions, maybe concealed by the siliciclastic contribution, during the latest Hauterivian–early Barremian in this part of the Cameros Basin (NW Iberian Range).

Acknowledgements This study was supported by the European Regional Development Fund and the Government of Aragón [Aragosaurus Group: Geological Resources and Palaeoenvironments, Grant number E18_20R] and the Spanish Ministry of Science, Innovation and Universities [Grant numbers RTI2018-093419-B-I00 and CGL2017-85038-P]. The authors acknowledge the use of the Servicio General de Apoyo a la Investigación-SAI of the University of Zaragoza. They would also like to thank C. Gallego for her advice during the FESEM sessions. E. Laita received a grant from the Government of Aragon for the development of her PhD. Our appreciation also goes out to the reviewers Dr. JF Deconinck and an anonymous reviewer to help us to improve the manuscript.

Author contributions All authors contributed to the study conception and design.

Funding Open Access funding provided thanks to the CRUE-CSIC agreement with Springer Nature. This study was supported by the European Regional Development Fund and the Government of Aragón [Aragosaurus Group: Geological Resources and Palaeoenvironments, Grant number E18_20R] and the Spanish Ministry of Science, Innovation and Universities [Grant number RTI2018-093419-B-I00].

Availability of data and material All data, materials and software application support the authors claims and comply with field standards.

Code availability Not applicable.

Declarations

Conflict of interest The authors have no conflicts of interest to declare that are relevant to the content of this article.

Ethical approval We confirm that the manuscript is original and is not being submitted to other journal.

Consent to participate Not applicable.

Consent for publication Not applicable.

References

Allix, P., Burnham, A., Fowler, T., Herron, M., Kleinberg, R., & Symington, B. (2011). Coaxing oil from Shale. *Oilfield Review, 22*(4), 4–15.

Aurell, M., Bádenas, B., Canudo, J. I., Castanera, D., García-Penas, A., Gasca, J. M., Martín-Closas, C., Moliner, L., Moreno-Azanza, M., Rosales, I., Santas, L., Sequero, C., & Val, J. (2019). Kimmeridgian-Berriasian stratigraphy and sedimentary evolution of the central Iberian Rift System (NE Spain). *Cretaceous Research, 102*, 1–19. https://doi.org/10.1016/j.cretres.2019.05.011

Aurell, M., Fregenal-Martínez, M., Bádenas, B., Muñoz-García, M. B., Élez, J., Meléndez, N., & de Santisteban, C. (2019). Middle Jurassic-Early Cretaceous tectono-sedimentary evolution of the southwestern Iberian Basin (central Spain): Major palaeogeographical changes in the geotectonic framework of the Western Tethys. *Earth-Science Reviews Science, 199*, 102983. https://doi.org/10.1016/j.earscirev.2019.102983

Aurell, M., Bádenas, B., Castanera, D., Gasca, J. M., Canudo, J. I., Laita, E., & Liesa, C. L. (2021). Latest Jurassic-Early Cretaceous synrift sedimentation of Torrelapaja Subbasin (Cameros Basin): Implications for Northeast Iberia palaeogeography. *Cretaceous Research, 128*, 104997. https://doi.org/10.1016/j.cretres.2021.104997

Bárdossy, G. (1982). *Karst Bauxites*. Elsevier.

Bauluz, B., Mayayo, M. J., Fernández-Nieto, C., & González López, J. M. (2000). Geochemistry of Precambrian and Paleozoic siliciclastic rocks from the Iberian Range (NE Spain): implications for source-area weathering, sorting, provenance, and tectonic setting. *Chemical Geology, 168*, 135–150. https://doi.org/10.1016/S0009-2541(00)00192-3

Bauluz, B., Yuste, A., Mayayo, M. J., & Canudo, J. I. (2014). Early kaolinization of detritalWeald facies in the Galve Subbasin (Central Iberian Chain, north-east Spain) and its relationship to paleoclimate. *Cretaceous Research, 50*, 214–227. https://doi.org/10.1016/j.cretres.2014.03.014

Biscaye, P. E. (1965). Mineralogy and sedimentation of recent deep-sea clay in the Atlantic Ocean and adjacent seas and oceans. *Geological Society of American Bulletin, 76*, 803–832.

Bodin, S., Fiet, N., Godet, A., Matera, V., Westermann, S., Clément, A., Janssen, N. M. M., Stille, P., & Fölmi, K. B. (2009). Early Cretaceous (late Berriasian to early Aptian) palaeoceanographic change along the northwestern Tethyan margin (Vocontian Trough, southeastern France): δ13C, δ18O and Sr-isotope belemnite and whole-rock records. *Cretaceous Research, 30*, 1247–1262. https://doi.org/10.1016/j.cretres.2009.06.006

Buscalioni, A. D., & Fregenal-Martínez, M. A. (2010). A holistic approach to the palaeoecology of Las Hoyas Konservat-Lagerstätte (La Huérguina Formation, Lower Cretaceous, Iberian Ranges, Spain). *Journal of Iberian Geology, 36*(2), 297–326. https://doi.org/10.5209/rev_JIGE.2010.v36.n2.13

Cantinolle, P., Didier, P., Meunier, J. D., Parron, C., Guendon, J. L., Bocquier, G., & Nahon, D. (1984). Kaolinites ferrifères et oxyhydroxydes de fer et d'alumine dans les bauxites des Canonettes (S.E. de la France). *Clay Minerals, 19*, 125–135.

Casas, A. M. (1993). Oblique tectonic inversion and basement thrusting in the Cameros Massif (Northern Spain). *Geodinamica Acta, 6*, 202–216. https://doi.org/10.1080/09853111.1993.11105248

Casas, A. M., Villalaín, J. J., Soto, R., Gil-Imaz, A., del Río, P., & Fernández, G. (2009). Multidisciplinary approach to an extensional syncline model for the Mesozoic Cameros Basin (N Spain). *Tectonophysics, 470*, 3–20. https://doi.org/10.1016/j.tecto.2008.04.020

Chamley, H. (1989). *Clay sedimentology*. Springer.

Clemente, P. (2010). Review of the Upper Jurassic-Lower Cretaceous Stratigraphy in Western Cameros basin, Northern Spain. *Revista De La Sociedad Geológica De España, 23*(3–4), 101–143.

Combes, P. J. (1990). Typologie, cadre géodynamique et genèse des bauxites françaises. *Geodinamica Acta, 4*(2), 91–109. https://doi.org/10.1080/09853111.1990.11105202

Dera, G., Pellenard, P., Neige, P., & Deconinck, J.-F. (2009). Distribution of clay minerals in Early Jurassic Peritethyan seas: palaeoclimatic significance inferred from multiproxy comparisons. *Palaeogeography, Palaeoclimatology, Palaeoecology, 271*, 39–51. https://doi.org/10.1016/j.palaeo.2008.09.010

Dhillon, S. K., & Dhillon, K. S. (1991). Characterisation of potassium in Red (Alfisols), Black (Vertisols) and Alluvial (Inceptisols and Entisols)) soils of India using electro-ultrafiltration. *Geoderma, 50*, 185–196.

Dinis, P. A., Carvalho, J., Callapez, P. M., Mendes, M. M., Santos, V. F., & Fernandes, P. (2020). Composition of Lower Cretaceous mudstones of the Algarve Basin and implications for Iberian paleoclimates. *Cretaceous Research, 110*, 104404. https://doi.org/10.1016/j.cretres.2020.104404

Do Campo, M., del Papa, C., Nieto, F., Hongn, F., & Petrinovic, I. (2010). Integrated analysis for constraining palaeoclimatic and volcanic influences on clay-mineral assemblages in orogenic basins (Palaeogene Andean foreland, Northwestern Argentina). *Sedimentary Geology, 228*, 98–112. https://doi.org/10.1016/j.sedgeo.2010.04.002

Do Campo, M., Bauluz, B., del Papa, C., White, T., Yuste, A., & Mayayo, M. J. (2018). Evidence of cyclic climatic changes recorded in clay mineral assemblages from a continental Paleocene- Eocene sequence, northwestern Argentina. *Sedimentary Geology, 368*, 44–57. https://doi.org/10.1016/j.sedgeo.2018.03.007

Ehrmann, W., Setti, M., & Marinoni, L. (2005). Clay minerals in Cenozoic sediments off Cape Roberts (McMurdo Sound, Antarctica) reveal palaeoclimatic history. *Palaeogeography*

Palaeoclimatology Palaeoecology, 229, 187–211. https://doi.org/10.1016/j.palaeo.2005.06.022

Fesharaki, O., García-Romero, E., Cuevas-González, J., & López-Martínez, N. (2007). Clay mineral genesis and chemical evolution in the Miocene sediments of Somosaguas, Madrid Basin, Spain. *Clay Minerals, 42*, 187–201. https://doi.org/10.1180/claymin.2007.042.2.05

Föllmi, K. B. (2012). Early Cretaceous life, climate and anoxia. *Cretaceous Research, 35*, 230–257. https://doi.org/10.1016/j.cretres.2011.12.005

Giovannini, A. L., Bastos Neto, A. C., Porto, C. G., Pereira, V. P., Takehara, L., Barbanson, L., & Bastos, P. H. S. (2017). Mineralogy and geochemistry of laterites from the Morro dos Seis Lagos Nb (Ti, REE) deposit (Amazonas, Brazil). *Ore Geology Reviews, 88*, 461–480. https://doi.org/10.1016/j.oregeorev.2017.05.008

Godet, A., Bodin, S., Föllmi, K. B., Vermeulen, J., Gardin, S., Fiet, N., Adatte, T., Berner, Z., Stüben, D., & Van de Schootbrugge, B. (2006). Evolution of the marine stable carbon-isotope record during the early Cretaceous: a focus on the late Hauterivian and Barremian in the Tethyan realm. *Earth and Planetary Science Letters, 242*, 254–271. https://doi.org/10.1016/j.epsl.2005.12.011

Godet, A., Bodin, S., Adatte, T., & Föllmi, K. B. (2008). Platform-induced clay-mineral fractionation along a northern Tethyanbasin-platform transect: implications for the interpretation of EarlyCretaceous climate change (Late Hauterivian-Early Aptian). *Cretaceous Research, 29*, 830–847. https://doi.org/10.1016/j.cretres.2008.05.028

Gómez-Fernández, J. C., & Meléndez, N. (1994). Estratigrafía de la Cuenca de los Cameros (Cordillera Ibérica Noroccidental, N de España) durante el tránsito Jurásico-Cretácico. *Revista De La Sociedad Geológica De España, 7*, 121–139.

Guerrak, S. (1987). Metallogenesis of cratonic oolitic ironstone deposits in the Bled el Mass, Azzel Mani, Ahnet and Mouydir basins, Central Sahara. *Geologische Rundschau, 76*, 903–922. https://doi.org/10.1007/BF01821072

Haywood, A. M., Valdes, P. J., & Markwick, P. J. (2004). Cretaceous (Wealden) climates: a modelling prospective. *Cretaceous Research, 25*, 303–331. https://doi.org/10.1016/j.cretres.2004.01.005

Hillier, S. (2003). Quantitative analysis of clay and other minerals in sandstones by X-ray powder diffraction (XRPD). *International Association of Sedimentologists Special Publication, 34*, 213–251.

Huggett, J. M., & Cuadros, J. (2005). Low-temperature illitization of smectite in the late Eocene and early Oligocene of the Isle of Wight (Hampshire basin), UK. *American Mineralogist, 90*(7), 1192–1202. https://doi.org/10.2138/am.2005.1674

Huggett, J. M., & Cuadros, J. (2010). Glauconite formation in lacustrine/palaeosol sediments, Isle of Wight (Hampshire Basin), UK. *Clay Minerals, 45*(1), 35–49. https://doi.org/10.1180/claymin.2010.045.1.35

Huggett, J. M., Gale, A. S., & Clauer, N. (2001). The nature and origin of non-marine 10 Å clay from the Late Eocene and Early Oligocene of the Isle of Wight (Hampshire Basin), UK. *Clay Minerals, 36*(3), 447–464.

Laita, E., Bauluz, B., Aurell, M., Bádenas, B., Canudo, J. I., & Yuste, A. (2020). A change from warm/humid to cold/dry climate conditions recorded in lower Barremian clay-dominated continental successions from the SE Iberian Chain (NE Spain). *Sedimentary Geology, 403*, 105673. https://doi.org/10.1016/j.sedgeo.2020.105673

Liesa, C. L., Soria, A. R., Casas, A., Aurell, M., Meléndez, N., Bádenas, B., Fregenal-Martínez, M., Navarrete, R., Peropadre, C., & Rodríguez-López, J. P. (2019). The South Iberian, Central-Iberian and Maestrazgo basins. In C. Quesada & J. T. Oliveira (Eds.), *The geology of Iberia: a geodynamic approach. Volume 5: active processes: seismicity, active faulting and relief* (pp. 214–228). Springer.

Mack, G., Calvin, W., & Curtis, H. (1993). Classification of paleosols. *Geological Society of America Bulletin, 105*, 129–136.

Martin, J. D. (2017). A software package for powder x-ray diffraction analysis. *Qualitative, Quantitative and Microtexture, 121*, 143.

Martín-Closas, C. (1989). *Els caròfits del Cretaci Inferior de les conques periferiques del Bloc de l'Ebre.* Ph.D Thesis. University of Barcelona

Mas, R., García, A., Salas, R., Meléndez, A., Alonso, A., Aurell, M., Bádenas, B., Benito, M. I., Carenas, B., García-Hidalgo, J. F., Gil, J., & Segura, M. (2004). Segunda Fase de rifting: Jurásico Superior-Cretácico Inferior. In J. A. Vera (Ed.), *Geología de España* (pp. 503–510). Sociedad Geológica de España-Instituto Geológico y Minero.

Mas, R., Benito, M. I., Arribas, J., Omodeo-Salé, S., Suarez-Gonzalez, P., Quijada, I. E., Guimerà, J., González-Acebrón, L., & Arribas, M. E. (2019). The Cameros Basin. In C. Quesada & J. T. Oliveira (Eds.), *The geology of Iberia: a geodynamic approach. Volume 5: active processes: seismicity, active faulting and relief* (pp. 190–205). Springer.

Meenakshi, Shrivastava, J. P., & Chandra, R. (2020). Pedogenically degenerated illite and chlorite lattices aid to palaeoclimatic reconstruction for chronologically constrained (8–130 ka) loess-palaeosols of Dilpur Formation, Kashmir, India. *Geoscience Frontiers, 11*(4), 1353–1367. https://doi.org/10.1016/j.gsf.2019.11.007

Mendelovici, E., Yariv, S. H., & Villalba, R. (1979). Iron-bearing kaolinite in venezuelan laterites: I. Infrared spectroscopy and chemical dissolution evidence. *Clay Minerals, 14*, 323–331.

Mestdagh, M. M., Vielvoye, L., & Herbillon, A. J. (1980). Iron in kaolinite: II. The relationships between kaolinite and iron content. *Clay Minerals, 15*, 1–13. https://doi.org/10.1180/claymin.1980.015.1.01

Michel, L. A., Tabor, N. J., & Montañez, I. P. (2016). Paleosol diagenesis and its deep-time paleoenvironmental implications Pennsylvanian-permian Lodève basin, France. *Journal of Sedimentary Research, 86*, 813–829. https://doi.org/10.2110/jsr.2016.41

Moiroud, M., Martinez, M., Deconinck, J. F., Monna, F., Pellenard, P., Riquier, L., & Company, M. (2012). High-resolution clay mineralogy as a proxy for orbital tuning: example of the Hauterivian-Barremian transition in the Betic Cordillera (SE Spain). *Sedimentary Geology, 282*, 336–346. https://doi.org/10.1016/j.sedgeo.2012.10.004

Molina, J. M., & Salas, R. (1993). Bauxitas kársticas del Cretácico inferior en Fuentespalda (provincia de Teruel): estratigrafía, origen y paleogeografía. *Cuadernos De Geología Ibérica, 17*, 207–230.

Mücke, A., Badejoko, A., & Akande, S. O. (1999). Petrographic-microchemical studies and origin of the Agbaja Phanerozoic Ironstone Formation, Nupe Basin, Nigeria: a product of a ferruginized ooidal kaolin precursor not identical to the Minette-type. *Mineralium Deposita, 34*, 284–296.

Mutterlose, J., & Ruffell, A. (1999). Milankovitch-scale palaeoclimate changes in pale–dark beddingrhythms from the Early Cretaceous (Hauterivian and Barremian) of eastern England and northern Germany. *Palaeogeography, Palaeoclimatology, Palaeoecology, 154*, 133–160.

Mutterlose, J., Bodin, S., & Fähnrich, L. (2014). Strontium-isotope stratigraphy of the Early Cretaceous (Valanginian-Barremian): Implications for Boreal-Tethys correlation and paleoclimate. *Cretaceous Research, 50*, 252–263. https://doi.org/10.1016/j.cretres.2014.03.027

Nkalih Mefire, A., Yongue Fouateu, R., Njoya, A., Mache, J. R., Pilate, P., Hatert, F., & Fagel, N. (2018). Mineralogy and geochemical features of Foumban clay deposits (west Cameroon): genesis and

potential applications. *Clay Minerals, 53*, 431–445. https://doi.org/10.1180/clm.2018.31

Nouazi Momo, M., Beauvais, A., Tematio, P., Ambrosi, J. P., Yemefack, M., Palmer Kfuban Yerima, B., & Yongue-Fouateu, R. (2019). Lateritic weathering of trachyte, and bauxite formation in West Cameroon: Morphological and geochemical evolution. *Journal of Geochemical Exploration, 205*, 106324. https://doi.org/10.1016/j.gexplo.2019.06.006

Platt, N.H. (1989). *Sedimentology and tectonics of western Cameros Basin. Province of Burgos. Northern Spain.* Ph.D. Thesis. University of Oxford

Price, G. D., Főzy, I., Janssen, N. M. M., & Pálfy, J. (2011). Late Valanginian-Barremian (Early Cretaceous) palaeotemperatures inferred from belemnite stable isotope and Mg/Ca ratios from Bersek Quarry (Gerecse Mountains Transdanubian Range, Hungary). *Palaeogeography, Palaeoclimatology, Palaeoecology, 305*, 1–9. https://doi.org/10.1016/j.palaeo.2011.02.007

Raucskik, B., & Varga, A. (2008). Climato-environmental controls on clay mineralogy of the Hettangian-Bajocian successions of the Mecsek Mountains, Hungary: an evidence for extreme continental weathering during the early Toarcian oceanic anoxic event. *Palaeogeography, Palaeoclimatology, Palaeoecology, 265*, 1–13. https://doi.org/10.1016/j.palaeo.2008.02.004

Reolid, M., Abad, I., & Martín-García, J. M. (2008). Palaeoenvironmental implications of ferruginous deposits related to a Middle-Upper Jurassic discontinuity (Prebetic Zone, Betic Cordillera, southern Spain). *Sedimentary Geology, 203*(1–2), 1–16. https://doi.org/10.1016/j.sedgeo.2007.10.001

Righi, D., & Meunier, A. (1995). Origin of clays by rock weathering and soil formation. In B. Velde (Ed.), *Origin and mineralogy of clays: clays and the environment* (pp. 43–161). Springer. https://doi.org/10.1007/978-3-662-12648-6_3

Rossi, C., & Cañaveras, J. C. (1999). Pseudospherulitic fibrous calcite in paleo-groundwater, unconformity- related diagenetic carbonates (Paleocene of the Ager basin and Miocene of the Madrid basin, Spain). *Journal of Sedimentary Research, 69*, 224–238. https://doi.org/10.2110/jsr.69.224

Saber, E. S., Ali, M., & El-Sheikh, A. (2018). Provenance studies of Kalabsha kaolin deposits, Egypt: a petrographical and geochemical approach. *Arabian Journal of Geosciences, 11*(339), 9. https://doi.org/10.1007/s12517-018-3690-4

Salas, R., Guimerà, J., Mas, R., Martín-Closas, C., Meléndez, A., & Alonso, A. (2001). Evolution of the Mesozoic central Iberian Rift System and its Cainozoic inversion (Iberian chain). *Peri-Tethys Memoir, 6*, 145–185.

Salas, R. (1987). *El Malm i el Cretaci inferior entre el Massís de Garraf i la Serra de'espadà. Anàlisi de conca*. Ph.D. Thesis, University of Barcelona

Schaetzl, R., & Thompson, M. L. (2015). *Soils: genesis and geomorphology*. Cambridge University press.

Schultz, L. G. (1964). Quantitative interpretation of mineralogical composition from X-ray and chemical data for the Pierre shale. *USGS Professional Paper, 391–C*, 1–131.

Scotese, C., Song, H., Mills, B. J. W., & Van der Meer, D. G. (2021). Phanerozoic paleotemperatures: the earth's changing climate during the last 540 million years. *Earth-Science Reviews, 215*, 103503. https://doi.org/10.1016/j.earscirev.2021.103503

Sheldon, N. D., & Tabor, N. J. (2009). Quantitative paleoenvironmental and paleoclimatic reconstruction using paleosols. *Earth-Science Reviews, 95*, 1–52. https://doi.org/10.1016/j.earscirev.2009.03.004

Smith, D. K., & Johnson, G. G., Jr. (2000). Digitized database quantification, DDBQ, analysis of complex mixtures using fully digitized patterns. *Advances in X-Ray Analysis, 42*, 276–286.

Steuber, T., Rauch, M., Masse, J. P., Graaf, J., & Malkoč, M. (2005). Low-latitude seasonality of Cretaceous temperatures in warm and cold episodes. *Nature, 437*, 1341–1344. https://doi.org/10.1038/nature04096

Tabor, N. J., Myers, T. S., & Michel, L. A. (2017). Sedimentologist's guide for recognition, description and classification of paleosols. In K. E. Zeigler & W. G. Parker (Eds.), *Terrestrial depositional systems: deciphering complexities through multiple stratigraphic methods* (pp. 165–208). Elsevier. https://doi.org/10.1016/B978-0-12-803243-5.00004-2

Varela, A. N., Raigemborn, M. S., Richiano, S., White, T., Poiré, A. G., & Lizzoli, S. (2018). Late cretaceous paleosols as paleoclimate proxies of high-latitude Southern Hemisphere: mata amarilla formation, patagonia, argentina. *Sedimentary Geology, 363*, 83–95. https://doi.org/10.1016/j.sedgeo.2017.11.001

Velasco, F., Herrero, J. M., Suárez, S., Yusta, I., Alvaro, A., & Tornos, F. (2013). Supergene features and evolution of gossans capping massive sulphide deposits in the Iberian Pyrite Belt. *Ore Geology Reviews, 53*, 181–203. https://doi.org/10.1016/j.oregeorev.2013.01.008

Velde, B. (1995). *Origin and mineralogy of clays: clays and the environment*. Springer.

Won, C., Hong, H., Cheng, F., Fang, Q., Wang, C., Zhao, L., & Churchman, G. J. (2018). Clay mineralogy and its palaeoclimatic significance in the Luochuan loess-palaeosols over ~1.3 Ma, Shaanxi, northwestern China. *Frontiers of Earth Science, 12*(1), 134–147. https://doi.org/10.1007/s11707-017-0625-4

Wright, V. P., Taylor, K. G., & Beck, V. H. (2000). The paleohydrology of Lower Cretaceous seasonal wetlands, Isle of Wight, Southern England. *Journal of Sedimentary Research, 70*, 619–632. https://doi.org/10.1306/2DC4092C-0E47-11D7-8643000102C1865D

Yuste, A., Bauluz, B., & Mayayo, M. J. (2015). Genesis and mineral transformations in Lower Cretaceous karst bauxites (NE Spain): climatic influence and superimposed processes. *Geological Journal, 50*, 839–857. https://doi.org/10.1002/gj.2604

Yuste, A., Bauluz, B., & Mayayo, M. J. (2017). Origin and geochemical evolution from ferrallitized Clays to karst bauxite: an example from the Lower Cretaceous of NE Spain. *Ore Geology Reviews, 84*, 67–69. https://doi.org/10.1016/j.oregeorev.2016.12.025

Yuste, A., Camacho, I., Bauluz, B., Mayayo, M. J., & Laita, E. (2020). Palaeoweathering events recorded on siliciclastic continental deposits (Albian, Lower Cretaceous) in NE Spain. *Applied Clay Science, 190*, 105598. https://doi.org/10.1016/j.clay.2020.105598